PAPER • OPEN ACCESS

Experimental and numerical Investigation of entrapped air presence and expulsions in irregular pipelines on hydraulic transients

To cite this article: H A Warda *et al* 2023 *J. Phys.: Conf. Ser.* **2616** 012014

View the article online for updates and enhancements.

Experimental and numerical Investigation of entrapped air presence and expulsions in irregular pipelines on hydraulic transients

H A Warda, E M Wahba and S I Elamrousy

Department of Mechanical Engineering, Alexandria University, Alexandria 21544, Egypt

E-mail: emwahba@yahoo.com

Abstract. In the present study, the transient event of rapid opening of upstream valve in undulated water pipeline with entrapped air pockets was investigated both experimentally and numerically. Pressure peaks and oscillation patterns were traced with the variation of air pocket length, blocking column length and water filling column. A transient two-dimensional CFD simulation model was introduced and validated by laboratory experiments. The proposed CFD model was conducted using ANSYS fluent based on Reynolds-averaged Navier– Stokes (RANS) equations and the volume of fluid (VOF) method. A user-defined functions (UDF) for both water compressibility effect and opening valve estimated pattern were adopted to verify the experimental results. For further understanding of transient response air expulsion through air vents of various orifices diameters were experimentally investigated. Image processing technique by using photoshop were utilized to clarify Stages of air expulsions, air water interaction and orifice flow regime. The obtained results showed that pressure peaks and oscillations depend strongly on orifice size where small orifice caused an intermitted flow choked by water column in contrast to large orifice where water hammer was dominated. An experimental facility was constructed at Alexandria university hydraulics laboratory to fulfil the research objectives. Air presence challenges in hydraulic systems are extensively applied for water and fuel supply lines, firefighting, and drainage systems in airports ground facilities.

1. Introduction

Hydraulic transients' events are triggered by a sudden disturbance in pipelines operating conditions. Rapid opening of upstream valve is one of the common conditions with a wide range of applications as in firefighting system, rainfall drainage system and urban flooding systems. Sometimes pipelines designers are obligated to follow an irregular configuration to avoid obstacles which coerce the air at pipe peaks to form air pockets, which sometimes could be beneficial or detrimental to pipeline system. Hydraulic failures associated by transients have been extremely costly in human lives and property Chaudhry [1]. For instance, in urban sewer drainage system, heavy rain could achieve full pipe flow accompanied by air entrapped because of the transition from open channel flow to closed conduit flow Li and Zhu [2], therefore, the suggestion of entrapped air in pipe irregular configuration is simulated to avoid or consider the unexpected pressure surge. Earlier researchers have investigated the propagations of pressure wave due to air entrapment in pipelines. Martin and CS [3] developed an analytical model describing the effect of presence of entrapped air in pipelines at line start-up his results showed that the form of air pocket could be critical specially near the dead end which induced more pressure surge.

Aktershev and Fedorov [4]examined hydraulic transients in a steel pipe having a cavity at the end of the pipe. Different volumes of cavity were used to fulfil the effect of volume of air on hydraulic transients and the results were validated numerically using the method of characteristics. Izquierdo, Fuertes, Cabrera, Iglesias and Garcia-Serra [5] developed a mathematical model to identify the peak pressure at pump start up in irregular profiled hydraulic system with multiple air pockets, their concluded that compressed air pocket between two water columns have a magnificent pressure surge. Fuertes, Cabrera, Izquierdo and Iglesias [6]studied the effect of liquid column variation on peak pressure due to air entrapped at horizontal pipe due to pump station start up. He theoretically used a rigid model instead of water hammer theory. Burrows and Qiu [7] has presented an analytical solution for pressure surge enhancement during pump shut down in the presence of air pocket. He concluded that the peak pressure is multiplied by 1.6 or 2 times the arising pressure, where large air cavity acts as a suppression for peak pressure on the contrary for small air cavity. Zhou, Liu and Ou [8] has investigated numerically and experimentally for one air pocket at end of pipe. his model was the first attempt to used VOF method which proved well agreement with experiments results to track air water interface during the transient event. Zhou, Liu and Karney [9] has experimentally investigated one air pocket in partially full water pipe. Variation of rising pressure, filling column and initial tail water were verified. He concluded that peak pressure is reduced in partial full pipe than in full air pipes. Zhou, Liu and Karney [9]performed an experiment and numerical investigation for rapidly filling of undulated pipeline containing two entrapped air pockets using multiple air pocket elastic water model. His results concluded that the most complicated case is the equal sized air pockets where the pressure surge could arise at both pockets and their interaction may cause huge pressure. The hydraulic systems subjected to rapid flow should get rid of air in a satisfactory manner to avoid pipe rupture. The air release during heavy rain events could cause geysers to manhole where water hammer is attained. Therefore, valves sizing for these systems is an important parameter to sustain undesired conditions. Holley [10] examined the surge induced due to the release of air entrapped at pipe when upstream valve was suddenly opened in water conveyance system. Huge pressure sure were recorded when air released at downstream vent. Albertson and Andrews [11] conducted theoretical and experimental studies on air expulsion from falling and rising pipeline. He recorded the maximum peak pressure which reached 15 times the operating pressure. De Martino, Fontana and Giugni [12] investigated experimentally the air expulsion through orifice at pipe downstream using different rising pressures and orifice diameters. He demonstrated the pressure oscillation pattern by two significant phases which are the low frequency for the air release stage and the high frequency for the water hummer effect when water column reached the orifice. Zhou, Pan, Wang, Liu and Wang [13] where rapid air-water through vertical pipe was analyzed experimentally. It was concluded that air release through orifice in vertical pipe undergoes two stages, the first pressurization, expansion then expulsion of air pocket and the second is the water hammer impact when water reaches the orifice as the air pocket length increases the pressure developed increase .Zhou, Hicks and Steffler [14] has investigated experimentally and analytically the rapid filling of a horizontal pipe with an orifice at the pipe end. Three pressure patterns have been observed depending on orifice size with no air release, small orifice, and large orifice. It was concluded that when the pipe has a dead end, or the orifice is small enough, the cushioning effect of air prevents the water column from impact on the pipe resulting in low pressure peaks. Apollonio, Balacco, Fontana, Giugni, Marini and Piccinni [15] carried out laboratory experiments to explain the effect of air expulsion at midpoint of undulating pipe. He stated that the ascending and descending slopes of irregular shaped pipe has a significant effect on hydraulic transients. Variations of upstream and downstream valves opening degree, orifices diameter and length of descending pipe are introduced. His results concluded that for larger orifices higher pressure surge is recorded with short descending slop. Zhou, Cao, Karney, Bergant, Tijsseling, Liu and Wang [16] have introduced an experimental and analytical investigation for air expulsion through horizontal end piped orifice. Details of air water pattern are investigated using image processing technique to identify the type of released flow whether its air, mist, water with little air or pure water with air volume variations and different orifice flow regimes. The experimental results showed at

smaller size orifice the maximum pressure reached 1.5 to 2 times of the inlet pressure whereas for the larger discharge orifice it reached up to nine times the inlet pressure.

Herein an experimental facility was constructed to explore the effect of the presence of one or more air pockets in irregular pipes by the variation of the amount of air, pocket location and blocking column length on hydraulic transients. In additional investigation of air release at three locations on the pipe with the variation of orifices sizes, amount of air and location of the expulsion. Two dimensional CFD model using ANSYS fluent is introduced to simulate two specified scenarios for one air pocket and two air pockets validated by experimental work in this study.
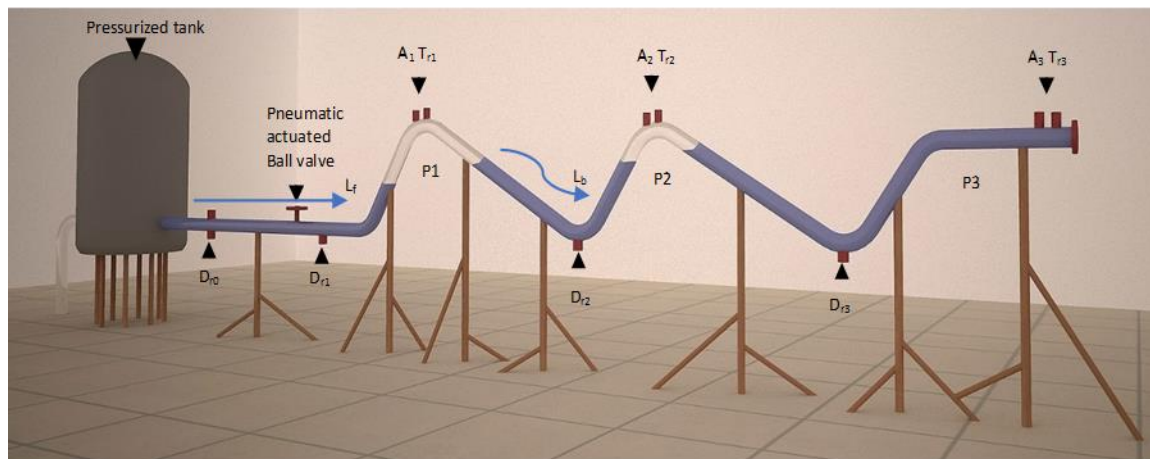

Figure 1. Experimental facility.

2. Experiment setup

The experimental facility (Figure 1) was constructed in the Fluid Mechanics and Hydraulic Machines Laboratory at Alexandria University and consists of a pressurized tank connected to a pipe 11.55 m long, 0.05 m diameter and 5 mm thickness. The pipe is made of 3.7 m straight PVC pipe divided into three flanged pipes and 7.85 m glass Perspex undulated flanged pipe. The exit pipe of the tank is equipped with a shutoff ball valve, pressure gauge, manual ball valve, pneumatically actuated ball valve and two water drains. The Perspex pipe is flanged and designed to hold two air pockets at the pipe peaks and at the end of the pipe. The pipe is equipped with three pressure transducers, three air valves and three water drains at each location. Three vents were installed at the pipe peak's locations with a provision to change their orifice size between four different sizes (1.5, 3, 5, and 7) mm diameter to investigate air expulsion from different orifice sizes at pipe peaks. Steel supports are used to rigidly fix the whole setup to the ground with rubber coated pipe hinges to hold the pipe. The three air pocket's locations are named as P1, P2 and P3 from the tank side. At each pocket location a pressure transducer is located (model FPA/060-C979-C8) that have a pressure scale from 0 to 200 PSIA. The DC voltage output ranges from 0 to 5 VDC while linearity range +/- 0.3% FS. A data-acquisition system is used to record output voltages from each transient signals. Agilent VEE v5.0 software is programmed to collect the data using a PC computer.

The rapid filling event is initiated electrically by energizing the pneumatically actuated ball valve which is connected to a pneumatic source at 7 bar to assure the fixed opening time of the ball valve which have been recorded in the captured videos to be approximately ranges between 0.08 secs to 0.09 secs.

3. Numerical approach

The numerical model goal is to simulate effect of the existence of air pocket in the closed conduit domain based on two-dimensional adopted by volume of fluid (VOF) method and shear-stress transport (SST)

turbulence model by solving Reynolds-Averaged Navier-Stokes equations (RANS) using ANSYS fluent software, where the (RANS) are for the 2-D form will be expressed as follows: -

$$\frac{\partial(\rho u)}{\partial t} + \nabla.(\rho u V) = -\frac{\partial P}{\partial x} + \nabla.(\mu \nabla \mu) + \left[-\frac{\partial(\rho \overline{u'^2})}{\partial x} - \frac{\partial(\rho \overline{u'v'})}{\partial y} \right] \qquad (1)$$

$$\frac{\partial(\rho v)}{\partial t} + \nabla.(\rho v V) = -\frac{\partial P}{\partial y} + \nabla.(\mu \nabla v) + \left[-\frac{\partial(\rho \overline{u'v'})}{\partial x} - \frac{\partial(\rho \overline{v'^2})}{\partial y} \right] \qquad (2)$$

Where the volume weighted average density and dynamic viscosity form are as follows: -

$$\rho = \alpha_v \rho_v + \alpha_l \rho_l \qquad (3)$$

$$\mu = \alpha_v \mu_v + \alpha_l \mu_l \qquad (4)$$

3.1. VOF model

When two fluid interactions are a point of interest the volume of fluid technique is the choice where the single sets momentum and volume equations of each fluid are solved throughout the domain. It was first published by Hirt and Nichols [17] as a numerical technique for tracking fluid phases interface as follows:-

3.1.1. VOF volume fraction equation. The two phases interface is tracked by the solution of the continuity equation of the volume fraction which has the following form: -

$$\frac{1}{\rho_q} \left[\frac{\partial}{\partial t}(\alpha_q \rho_q) + \nabla.(\alpha_q \rho_q \vec{v}_q) = S_{\alpha_q} + \sum_{p=1}^{n}(\dot{m}_{pq} - \dot{m}_{qp}) \right] \qquad (5)$$

3.1.2. Time discretization implicit scheme. The time discretization method is used in the implicit scheme for the stability of the numerical solution of the two-phase flow to calculate the face fluxes of all cells involving the cells near wall. ANSYS Fluent's default quick, second Order Upwind and First Order Upwind, and the Modified HRIC schemes were the implicit form as follows:

$$\frac{\alpha_q^{n+1}\rho_q^{n+1} - \alpha_q^n \rho_q^n}{\Delta t} V + \sum_f (\rho_q^{n+1} U_f^{n+1} \rho_{qf}^{n+1}) = \left[S_{\alpha_q} + \sum_{\rho=1}^{n}(\dot{m}_{\rho q} - \dot{m}_{q\rho}) \right] V \qquad (6)$$

3.1.3. Shear-stress transport (SST) k-ω turbulence. The Shear-stress transport (SST) k-ω turbulence was chosen as turbulence model due to several reasons as it combines the advantage of the standard k-ω model at near wall region and advantage of the k-ε model at the far field in the following form: -

$$\frac{\partial}{\partial t}(\rho k) + \frac{\partial}{\partial x_i}(\rho k u_i) = \frac{\partial}{\partial x_j}(\Gamma_k \frac{\partial k}{\partial x_j}) + G_k - Y_k + S_k \qquad (7)$$

And

$$\frac{\partial}{\partial t}(\rho \omega) + \frac{\partial}{\partial x_j}(\rho \omega u_j) = \frac{\partial}{\partial x_j}(\Gamma_\omega \frac{\partial \omega}{\partial x_j}) + G_\omega - Y_\omega + D_\omega + S_\omega \qquad (8)$$

Where G_ω represents the generation of ω and G_k represents the production of turbulence kinetic energy.

3.2. User defined functions (UDF)

Two UDFs were introduced in the numerical simulation in ANSYS fluent for the calculation of the density of the liquid phase where the gas phase is determined by ideal gas law and the second UDF for the cubic polynomial equation of the ball valve opening to fit the actual valve opening scheme. The density is calculated by the known liquid density at reference pressure and the speed of sound for the liquid phase (400 m/sec determined from Zhou, Liu and Karney [9]). where the speed of sound for liquid phase are in the following form: -

$$a_l = \sqrt{\frac{k_l/\rho_l}{1+\left[\frac{k_l D}{E\,e}\right]}} \approx \sqrt{\frac{k_{eq}}{\rho_{lo}}} \qquad (9)$$

By substituting the value of k_{eq} in the following form: -

$$\rho_l = \rho_{lo}\left(1 + \frac{P-P_o}{k_{eq}}\right) \qquad (10)$$

Where a_l is the speed of sound, ρ_{lo} is the liquid phase density at reference pressure (P_o), E is the young modulus of elasticity of the pipe, k_l is the liquid phase modulus of elasticity, D is the pipe diameter, e is the pipe thickness.

4. Results and discussions

The hydraulic transient effect of the rapid filling of the air pocket existence are explored experimentally for one or two air pockets associated with variation of air pocket length, blocking column length and air pocket location as well as the expulsion of air at different locations with different orifice diameters (1.5,3,5 and 7 mm). The driving pressures of the tank (H $_d$) conducted are (1.6 bar & 2 bar) and the filling water column length (L $_f$). The aim of this study is the peak pressure estimation, and the pressure oscillation patterns therefore photo processing technique is utilized to visualize the air-water interactions as well as the compression and retraction stages of the air pockets on the time frame where photoshop program is used to divide the captured videos into frames to fully understand the phenomena of air expulsion.

4.1. One air pocket scenario

As mentioned in earlier studies the one air pocket scenario has already been investigated. However, At the beginning of this study a simple experiment of one air pocket was conducted to help interpreting the pressure oscillation patterns and understanding the different stages of compression and expansions of air pocket process during the transient event until it reaches the equilibrium state. Table (1) lists selected cases of the one entrapped air pocket associated with factors such as filling water column length and air pocket length. Experiment#5 was selected specifically for the purpose of numerical model verification. To help explaining the transient pressure pattern the air pocket movement was visualized and photographed during transients. Figure 5(a-e) illustrates the first cycle of the repeated compression and expansion wave in which the filling column moved forward in the pipe acting as a mechanical piston compressing the air pocket where the blocking column behaves like a dead end. The peak pressure always takes place in the 1st cycle at different wave amplitudes and frequency depending on the flow conditions.

Table 1. List of one air pocket experiments.

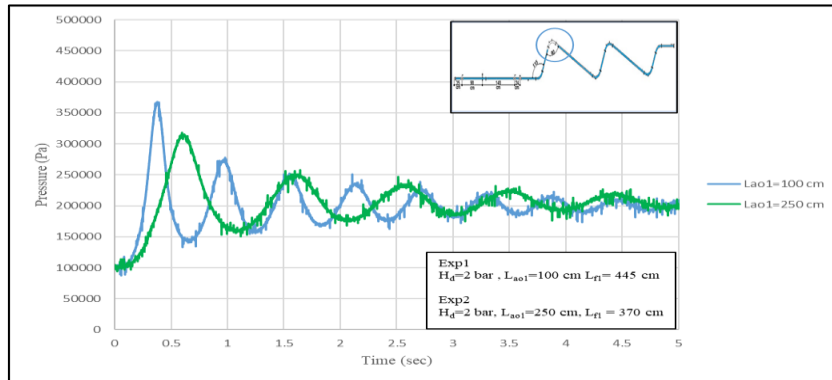| #	Driving head (H $_d$) Bar	Pocket location	Length of air pocket (L$_{ao1}$) cm	Filling column length (L $_f$) cm	Measuring Transducer
1	2	Pocket 1	100	445	T$_{r1}$
2	2	Pocket 1	250	370	T$_{r1}$
3	2	Pocket 2	250	695	T$_{r2}$
4	2	Pocket 3	100	970	T$_{r3}$
5	1.6	Full pipe	863	289	T$_{r3}$

Figure 2. One air pocket Experiment # (1,2) at pocket 1.
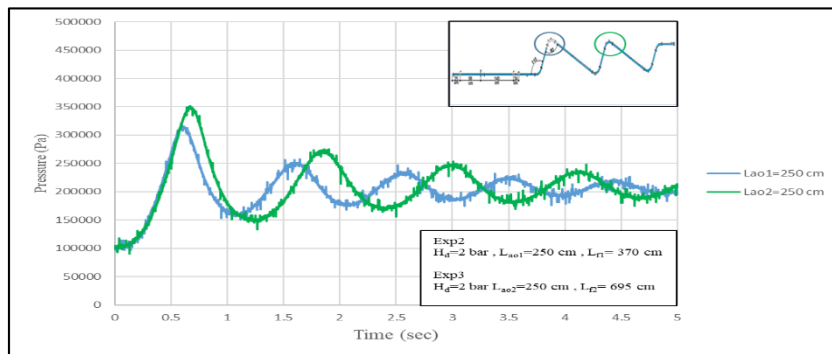

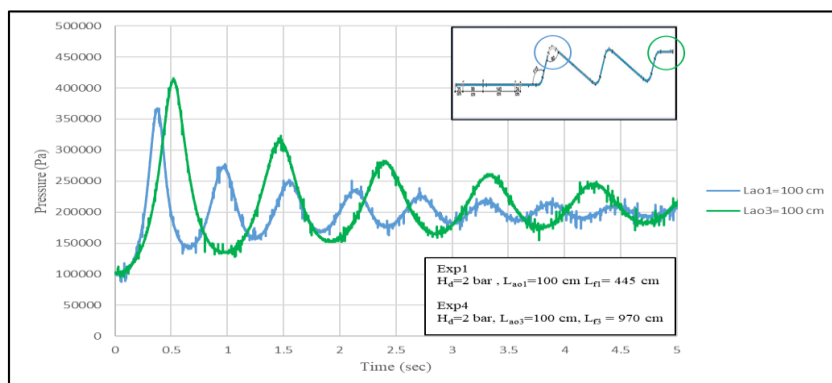**Figure 3**. One air pocket Experiment # (2,3) at pocket 1 & pocket 2.

Figure 4 .One air pocket Experiment # (1,4) at pocket 1 & pocket 3.
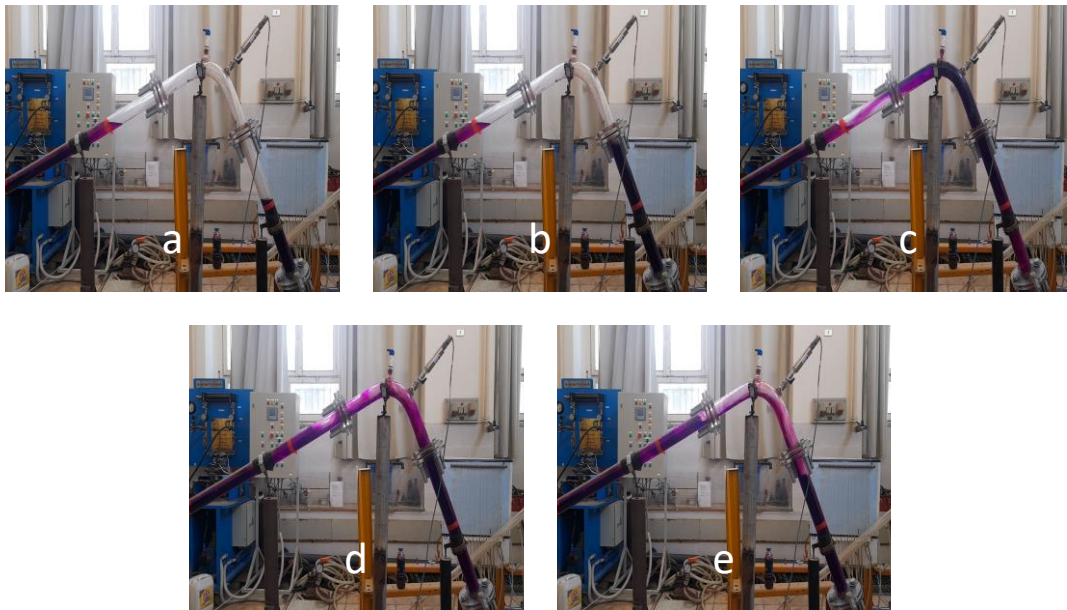
Figure 5 .One air pocket stages illustration during transient.
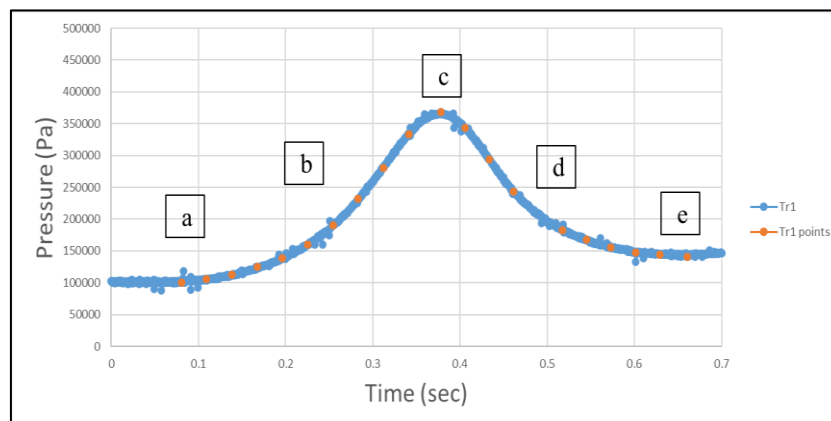

Figure 6. One air pocket Experiment #1 first cycle of air pocket -water interactions.

Figure 2 illustrates the effect of air pocket size on hydraulic transients where two distinct pockets lengths (250 cm & 100 cm) are positioned at the same location (Pocket 1). The pressure rise in case of the smaller pocket is steeper with higher peak and higher frequency compared to the case of the bigger pocket where the cushioning effect dampens the pressure wave causing a delayed pressure to rise with a lower amplitude. Figure 3 illustrates the effect of filling column length on hydraulic transients where the same pocket sizes (250 cm) are located at two different positions (Pocket 1 and pocket 2). It was observed that the peak pressure always occurs at the pocket 2 with longer filling column length due to its higher inertia. Figure 4 illustrates the effect of filling column length on hydraulic transients where the same pocket sizes (100 cm) are located at two different locations (Pocket 1 & pocket 3) which are further apart. It was observed that the peak pressure is further increased at pocket 3 due to the longer filling column with higher inertia. The longer filling column length takes longer time to retract and consequently the oscillation frequency is lower. Figure 5 illustrates the main stages of air water interaction mechanism in details where each frame has its corresponding point on pressure oscillation in Figure 6 as follows: - Figure 5(a) described the initial state just after valve opening. Figure 5(b) shows

midpoint of the compression stage where the air pocket length starts to decrease by the advancement of the filling column, while Figure 5(c) presents the end of the compression stage and the starting of the expansion stage indicated by the peak pressure reached where the air pocket reached its minimum size. Figure 5(d) describes the midpoint of the refraction stage where the pocket starts to expand occupying larger space. Figure 5(e) described the end of expansion at the end of the 1st cycle of the pressure wave oscillation.

4.2. Two air pockets scenario

The phenomena of two air pockets are more complicated than one air pocket as the blocking water column moves freely forward and backward between the two pockets due to air compressibility. The three locations (P1- P2-P3) were selected to explain the effect of variation of the two air pocket sizes and blocking column lengths using various air pocket lengths. One of the experiments is selected for numerical validation which will be introduced later in section 4.3.

4.2.1. Effect of two air pocket sizes on hydraulic transients. In this section the effect of changing downstream pocket size on pressure transients for small and large upstream pocket size were shown in Figures 7 & 8. Figure7 illustrated the small upstream air pocket length (Lao1=25cm) with various downstream pocket sizes (Lao2=100-50-25 cm), where the compressibility of the large size downstream pocket in Figure 7(a) delayed its time to compress for the 1st cycle while the upstream pocket undergoes more cycles of compression and expansion before it reaches the maximum pressure peak with lower frequency. As the downstream pocket size decrease in size as in Figure 7(b) and Figure (7c) the less delay time at the fist cycle, the less cycles of compression and expansions while higher frequency recorded during the same period. It was also observed that the highest pressure was inversely proportional to the downstream pocket size which reached more than twice the driving pressure for equal sized pockets as shown in Figure 7(c). Figure 8 illustrates the case of big upstream air pocket size (Lao1=100cm) with various downstream pocket sizes (Lao2=25-50-100). It is observed that the large size of the upstream pocket absorbs the filling column impulse which smoothens out the pressure pattern for smaller downstream pocket as in Figure 8(a), where both upstream and downstream patterns started together with no delay and higher frequency. As the downstream pocket size increases the downstream pocket pattern delay increases and the more cycles of compressions and expansions with noticeable decrease in the wave frequency as shown in Figure 8(b) & Figure 8(c), where the highest pressure decreased with the increase in downstream pocket size. It was reviewed from literature Zhou, Liu [9] and concluded from experimental observations that three remarkable situations occurred defined by the pressure peak location nearly the same blocking column lengths, although it has a significant effect on peak pressure location which will be discussed later in section 5.2.2.

1- When the upstream pocket length (L_{ao1}) is much smaller than the downstream (L_{ao2}) the pressure peak is probably act at the upstream pocket.

2- When the upstream air pocket length (L_{ao1}) is much bigger than the downstream (L_{ao2}) the pressure peak always acts on the downstream pocket.

3- When the two air pockets' lengths are equal in size and smallest, the maximum pressure occurs in the two pockets almost simultaneously and represents the worst case.
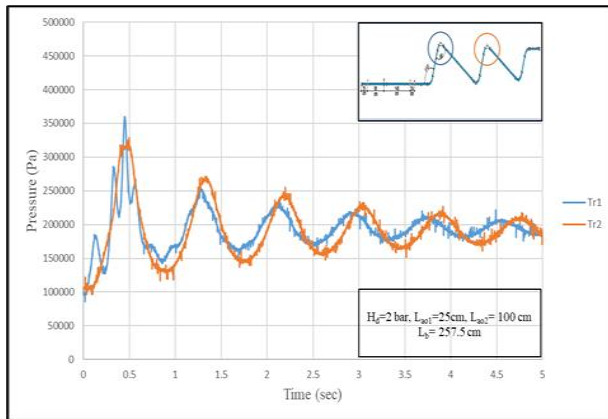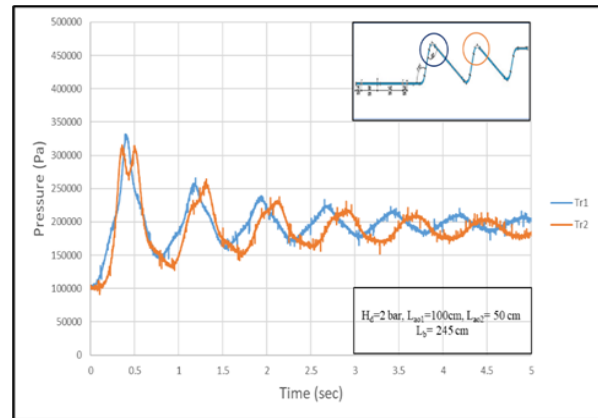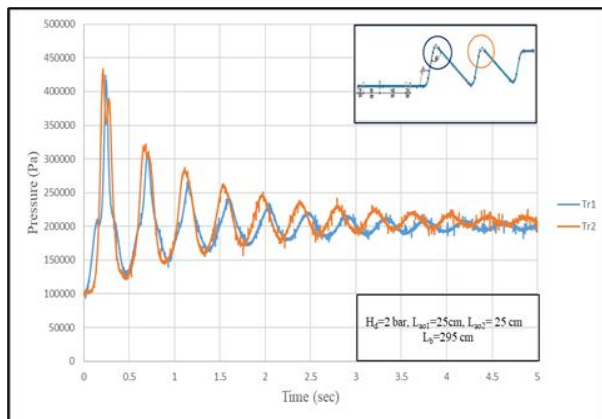
(a) L_{ao1}=25 cm, L_{ao2}= 100 cm.
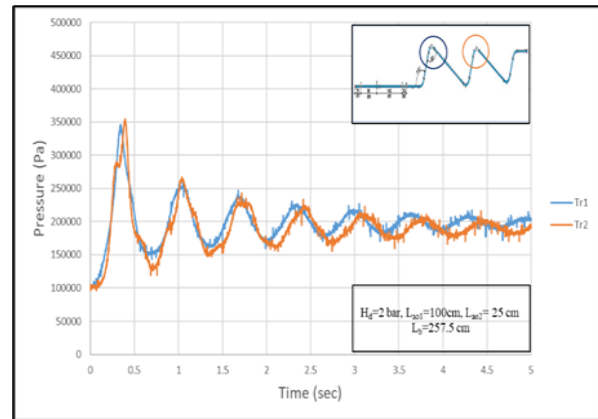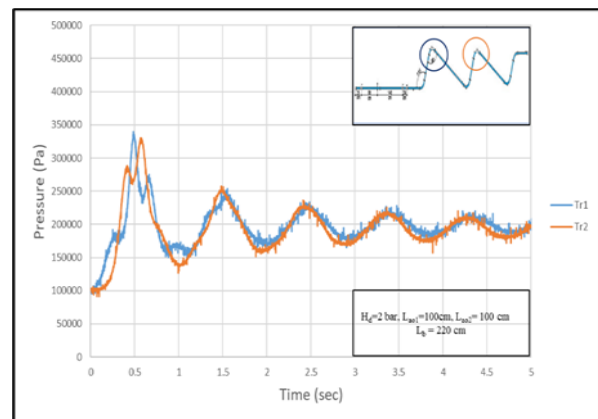

(a) L_{ao1}=100 cm, L_{ao2}=25 cm.
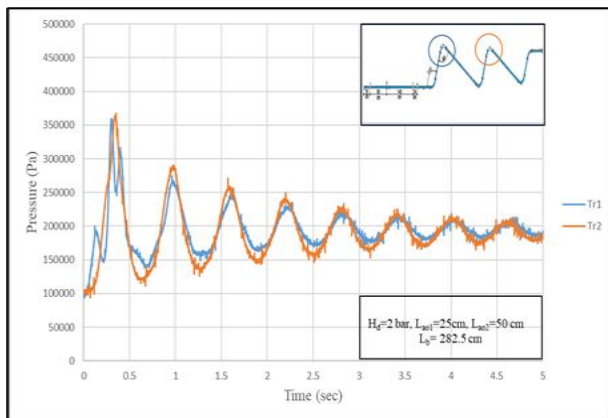
(b) L_{ao1}=25 cm, L_{ao2}= 50 cm.

(b) L_{ao1}=100 cm, L_{ao2}= 50 cm.

(c) L_{ao1}=25 cm, L_{ao2}= 25 cm.

(c) L_{ao1}=100 cm, L_{ao2}=100 cm.

Figure 7. Effect of small size upstream pocket (25 cm) with various sizes of downstream pocket (25-50-100).
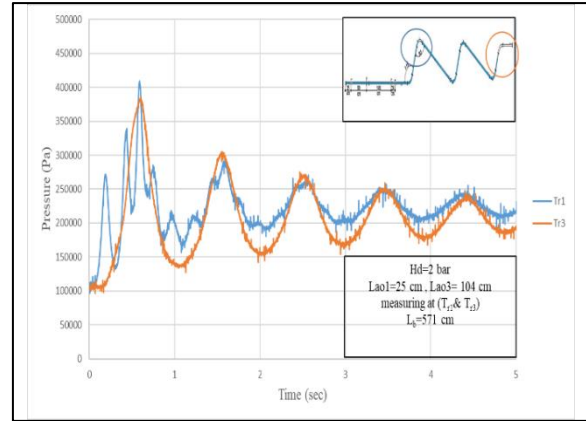
Figure 8. Effect of big size upstream pocket (100 cm) with various sizes of downstream pocket (25-50-100).

4.2.2. Effect of Two air pockets blocking column variations on hydraulic transients. In this section a set of six experiments were conducted to explain the blocking column length variation effect. Three air pocket size ratios are used (0.24,1&4.15) as a fixed parameter with short and long blocking column lengths. During transients, advancing the filling column causes the blocking column to move forward and backward between the two air pockets due to air compressibility. The movement of the filling and blocking columns with respect to each other decide the behaviour of the air pockets pressure oscillations and the occurrence of the maximum pressure. When they moved together in the same direction the upstream pocket is expanded causing pressure decrease while when they moved in opposite directions, the upstream air pocket is compressed causing its pressure to rise. Meanwhile, the blocking column is considered as a filling column of the downstream pocket causing its pressure to rise further due to the column's inertia. Figure 9 illustrates the Pressure oscillations results for small ratio of air pockets lengths (L_{ao1}/L_{ao2}=0.24) where the upstream pocket is too small compared to the downstream one. When the blocking column is short (L_b=212.5cm) its inertia is relatively small where both pockets compress and retract together causing the same pressure amplitude in both pockets where the bigger size of the downstream pocket takes longer time to compress delaying the reflection of its pressure wave resulting in an increased number of compressions and expansions stages during the first cycle in the upstream pocket, and consequently both pressure traces propagate with a lower frequency as shown in Figure 9(a). On the other hand, for longer blocking column (L_b =571cm) as shown in Figure 9(b) it was observed that due to the high blocking column inertia the pressure in the second pocket rises much faster with a significant rise in peak pressure, resulting also in a higher frequency of the pressure pattern of both upstream and downstream air pockets. Figures 10-11 illustrate the effect of the blocking column length for other different air pocket column length ratios confirming the above findings, namely increased peak pressure values at air pocket's locations due to the higher inertia of the blocking column and that peak pressure occurs earlier at both pockets. Meanwhile, as the second trapped air pocket gets relatively very short (25 cm) the extent of peak pressure rises in the downstream trap getting much higher. On the other hand, as the upstream air pocket length gets longer with respect to the length of downstream air trap the number of compressions and expansions stages during the first cycle in the upstream air pocket disappears, as shown in Figure 10(a) & Figure 11(a). It is also observed that in all cases, as the blocking column length gets longer and due to its higher inertia the second air trap gets compressed faster and consequently the frequency of the pressure pattern increases. Zhou, Liu and Karney [9]in developing there multiple-air-pocket elastic-water model considering multiple moving boundaries of water columns, there studies revealed three types of pressure oscillation patterns, associated with blocking column length and air length ratio ($L_{a01}=L_{a02}$), in which they related these types to the occurrence location of the maximum pressure; (1) Type1: pressure histories of the two air pockets are in good agreement, namely, $H_{max} = H_{ao1}=H_{ao2}$ (2) Type 2: the highest pressure arises in the upstream air pocket, namely $H_{max} = H_{ao1}>H_{ao2}$. (3) Type 3: the maximum pressure value occurs within the downstream air pocket, namely, $H_{max} = H_{ao2}>H_{ao1}$. It was interesting to note that their classification of type 3 agrees with the above experimental findings in which when the blocking column is long and the downstream pocket is small, the maximum pressure of the downstream air pocket is much higher than the upstream air pocket (Type 3). One explanation is that the blocking column can be treated as the filling column for the downstream air pocket and that the small air pocket is prone to cause higher pressure.

Meanwhile, same agreement occurs for type 1, where when the upstream air pocket with a length sufficiently lower than the downstream air pocket, as shown in Figure 9(a), when the blocking column is very short, the inertia can be ignored, and the two air pockets are almost compressed and expanded synchronously namely, $H_{max} = H_{ao1}=H_{ao2}$.
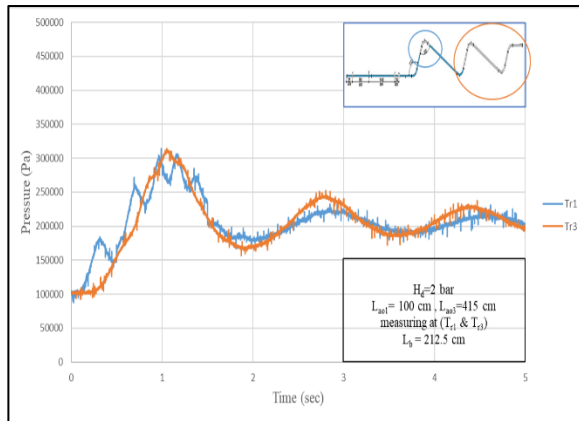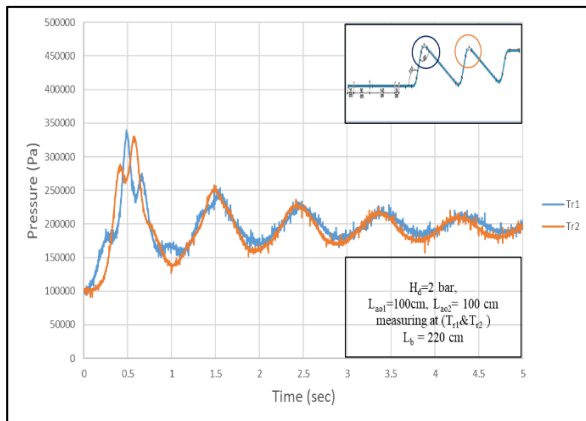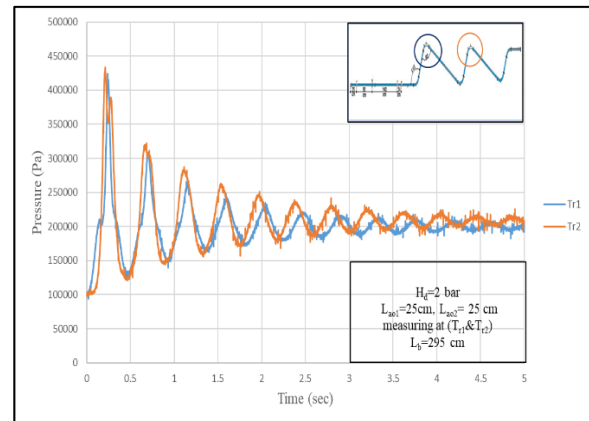
(a) Short blocking column (L_b=212.5 cm).   (b) Long blocking column (L_b=571 cm).

Figure 9. Small air pockets ratio, (L_{ao1}/L_{ao2} =0.24) for short and long blocking column.
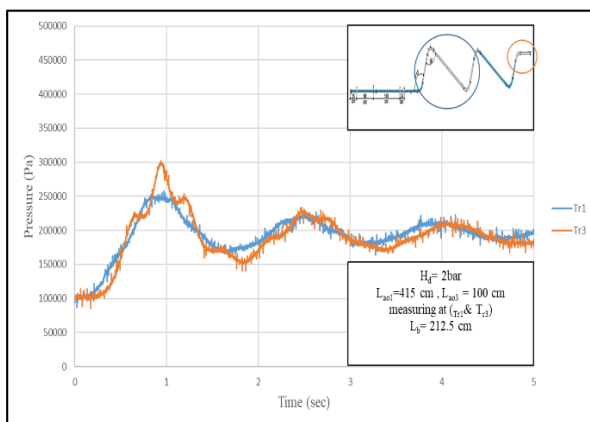

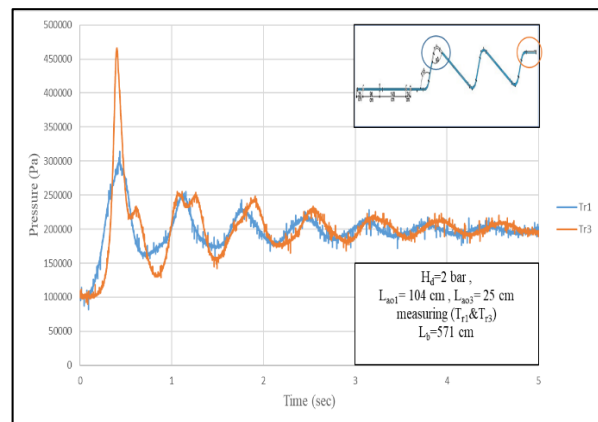(a) short blocking column (L_b=220 cm).   (b) Long blocking column (L_b=295 cm).

Figure 10. Equal air pocket ratio (L_{ao1}/L_{ao2}=1) for short and long blocking column.

(a) Short blocking column (212.5 cm).   (b)Long blocking column (L_b=571cm).

Figure 11. Big air pocket ratio (L_{ao1}/L_{ao2} =4.15) for short and long blocking column.

4.3. Model verification

The comparison between the laboratory results and the CFD simulated results for two cases were verified with good agreements. Figure 12 showed the validation for one air pocket case where the whole pipe is considered a huge air pocket. When the valve is opened the filling column undergo a continues preceding through the pipe length compressing the air volume till it reached its minimum compressed volume then the spring effect of air caused forward and backward movement between the two phases till the whole system reached the equilibrium state. Figure 13 illustrated the two distinct air pockets case where the upstream air pocket with huge size (L_{ao1}=605 cm) and downstream with smaller size (L_{ao2}=50 cm). when the valve is opened both air pockets started to move toward the pipe end where the two pockets started to compress together specially the second pocket which fully diminished by two phase interaction as the preceding of the blocking column act as the filling column for it. it was recorded that the maximum pressure arises at the second air pocket. The proposed model could estimate the pressure peak which is the key factor for pipeline safety designs well as the pressure pattern which showed well match specially for the first cycle.
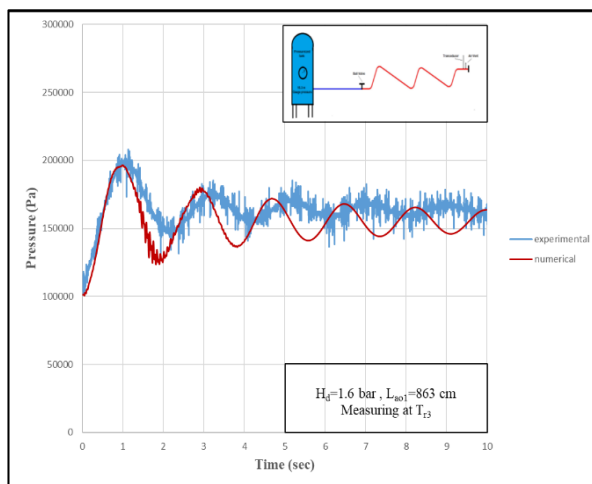

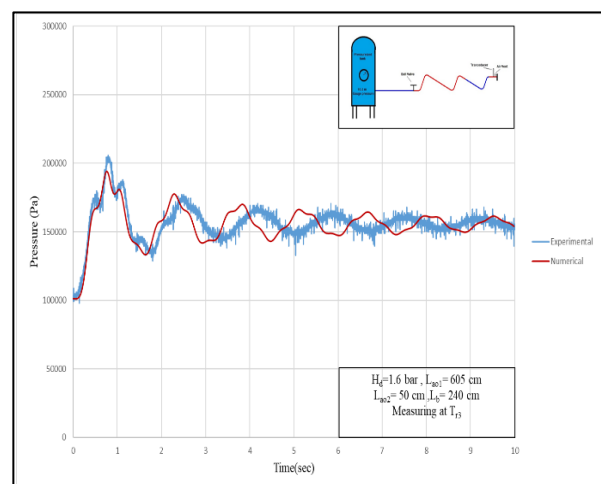**Figure 12.** One air pocket numerical and experimental results comparison

Figure 13. Two air pockets numerical and experimental results comparison.

4.4. Expulsion experiments results

The air release or expulsion behavior was studied to complete the understanding of transient event during the air pocket process to exit the pipe. The movement of the air is monitored in each process before the water column reaches the orifice depends mainly on the orifice size as well as other flow conditions. Therefore, four orifices' sizes (1.5-3-5-7 mm) at each pocket locations (P1, P2&P3) are used to perform a total of 36 experiments. The amount of air pocket is considered for each pocket location to show its effect. Image processing technique is used to visualize the air pocket movements, air-water interactions, and orifice flow regime.

4.4.1. Effect of orifice size on pressure surge during air expulsion. Figures (14-17) illustrate pressure oscillation as a result of air expulsion from four different orifices sizes (d_0=1.5-3-5-7 mm). The location (P3) was selected using fixed value of air pocket (L_{ao3}=50cm) in the four cases
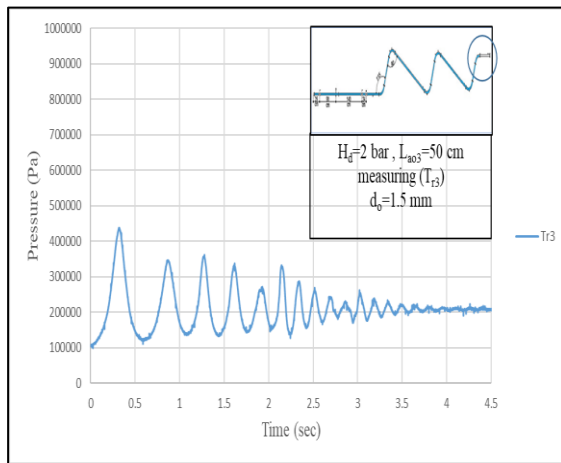
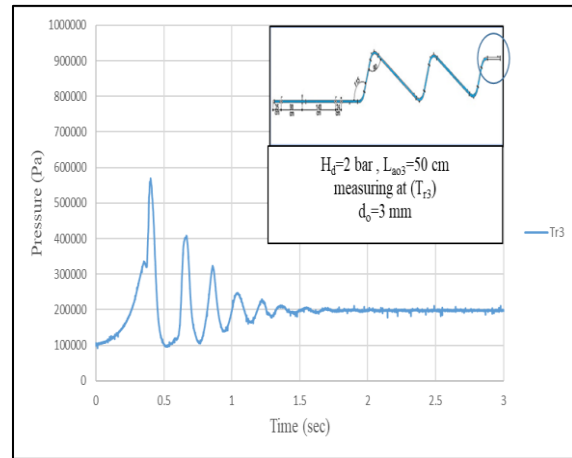**Figure 14**. Air pocket expulsion at pocket 3 (L_{ao3}=50 cm, d_o=1.5 mm).

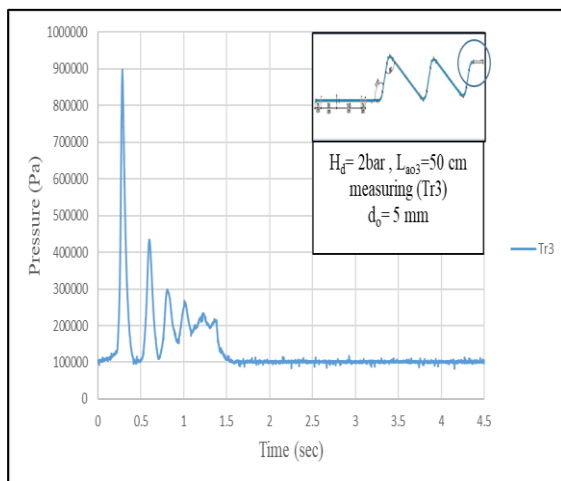**Figure 15**. Air pocket expulsion at pocket 3 (L_{ao3}=50 cm, do=3 mm).

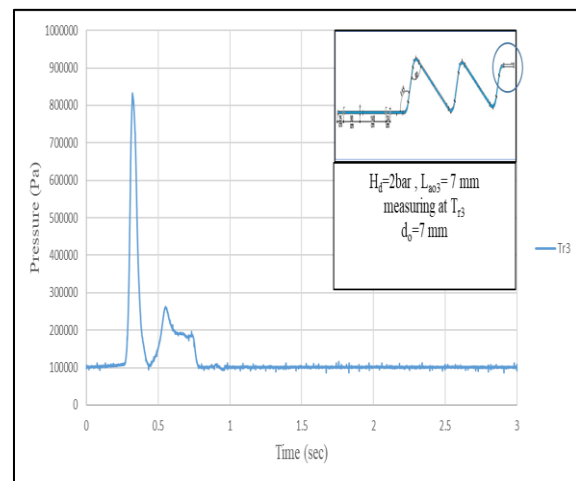**Figure 16**. Air pocket expulsion at pocket 3 (L_{ao3}=50cm, d_o=5 mm).

Figure 17. Air pocket expulsion at pocket 3 (L_{ao3}=50 cm, d_o=7 mm).

Figure14 illustrated the pressure pattern when the orifice diameter is exceedingly small (1.5mm). The air pocket starts to compress gradually to reach the peak pressure before the water column reaches the orifices during the compression stage. The cushioning effect of air decreases the water impact on the orifice. An intermittent air and mist expel through the orifice till all air is released from the pipe. Figure 15 illustrated the pressure pattern when the orifice is medium size (3mm) where the peak pressure records significant increase more than that with smaller orifice which happened directly after the water column hits the orifice during the compression stage of residual air. Figure 16 for larger orifice diameter (5mm) showed an obvious water hammer effect where the highest recorded peak pressure is reached at the water column impact with noticeable loud voice where air is released without any cushion effect of air. Figure17 showed for more larger orifice diameter (7mm) the same pressure rises due to water hammer where the orifice become more bigger than (5 mm) which is considered the critical orifice size where the water slam is decreased due to the orifice size resulted in decreasing the water column impact that reduce the pressure rise. Here is a graph shows the relation between orifice size and pressure peaks. As shown in Figure 18.
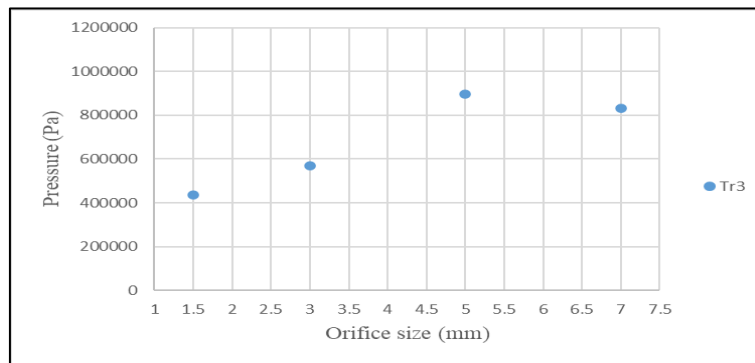
Figure 18. Peak pressure vs orifice size at pocket 3.

4.4.2. Effect of pocket size on pressure surge during air expulsion. The amount of air in the pocket has a significant effect on peak pressure as well as the time required for the full air expulsion. Figure 19 showed the highest peak pressure arises at small size pocket as the cushion effect is the lowest on the other hand when the pocket size increases the compression stage takes longer attenuating the pressure to lower value.
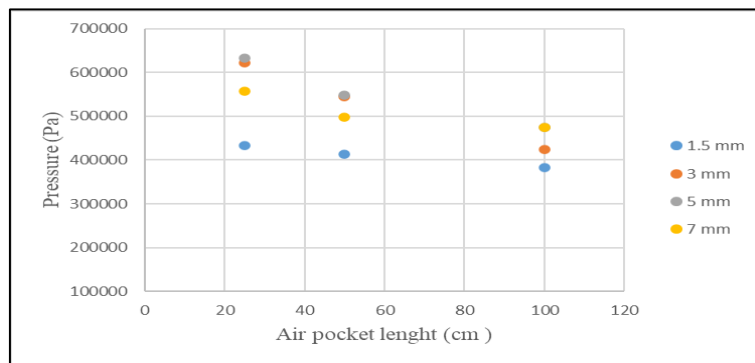

Figure 19.Air pocket length vs peak pressure at pocket 2.

4.4.3. Effect of pocket location on pressure surge during air expulsion. The selection of the air pocket location affects the peak pressure as the water column length increase with more inertia force which produces more pressure increase clearly shown in Figure 20 where air expulsion is performed at three pocket locations (P1, P2& P3) with orifice diameter (d_o=5 mm) & air pocket length (L_{ao}=50cm) the highest-pressure surge for air expulsions at pocket 3 (P3) with the longest water column.
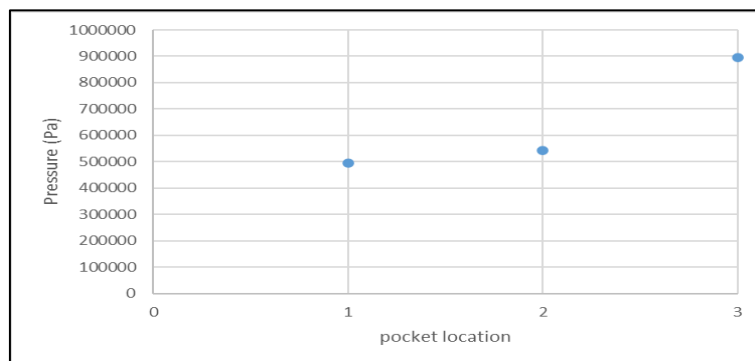

Figure 20. Air pocket location vs peak pressure.

4.4.4. Image processing technique for air expulsions. In this section the technique of image processing was used by using Photoshop software to divide the experiments captured videos in frames to express the Stages of air expulsion illustrated in pictures for every significant change in flow regime. Three different orifices were used (1.5, 3 & 7) mm each one had its own transient response. At the beginning the setup of two air pockets at Figure21 was fitted with orifice (1.5 mm) at the pipe end (T_{r3}) where the pressure oscillation recorded and analysed to determine the type of flow regime at orifice nozzle. Each regime was highlighted by colours on the pressure oscillation against time domain as shown in following figure: -
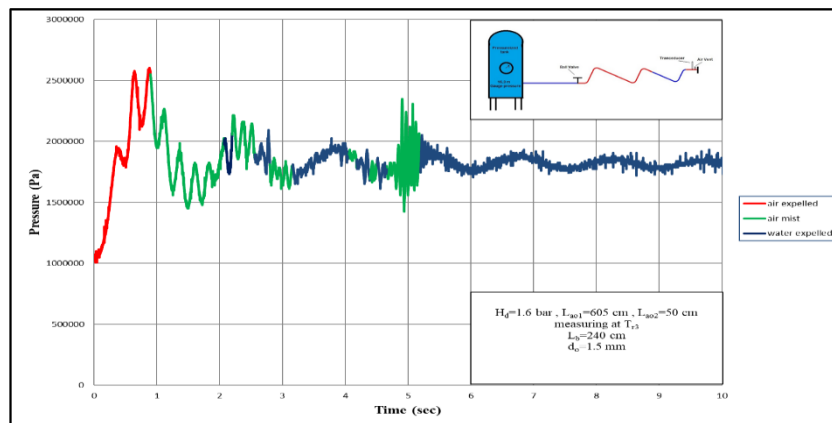

Figure 21. Stages of Air expulsion through 1.5 mm orifice at pocket 3.

Figure21 showed that the process of air release through orifice size (d_0=1.5mm) at pocket 3 with two air pocket configuration (L_{ao1}=605 cm and L_{ao2}=50 cm) with driving tank pressure (H_d=1.6 bar).it was observed the first stage (red colour) represents the air release for nearly 1 sec after that the second stage (green colour) represents intermitted mist release combined with water release (blue colour) for almost 5.2 secs then the third stage represents the water expelled (blue colour) for the rest of the period.
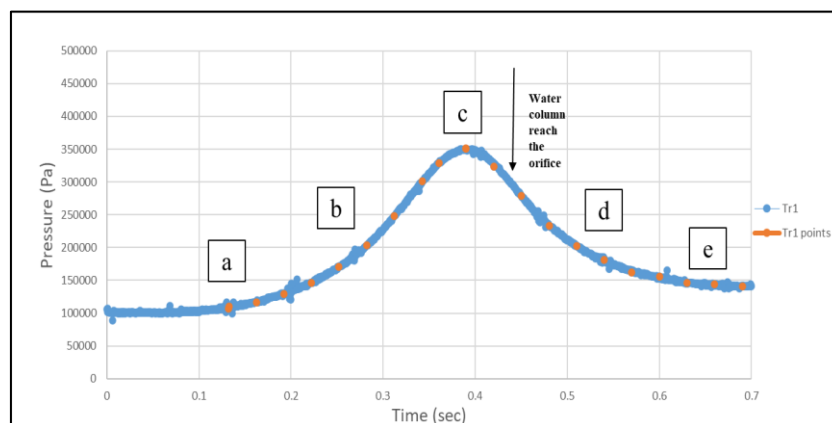

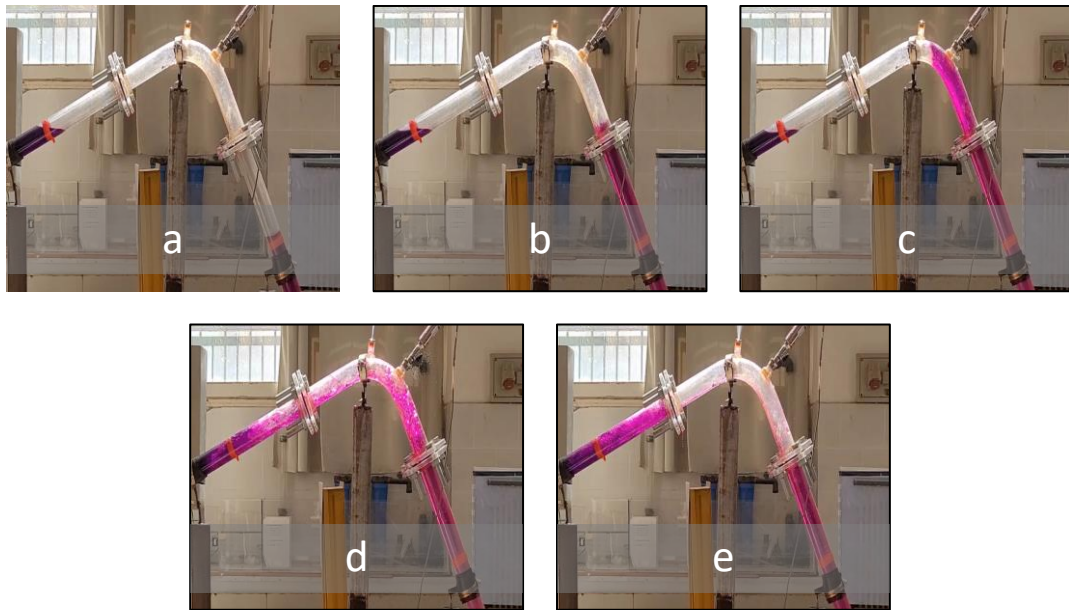**Figure 22**. 1st cycle of air expulsion at P1 (d_o=1.5 mm).

Figure 23. illustration of air pocket expulsion at pocket 1 (d_o=1.5 mm).
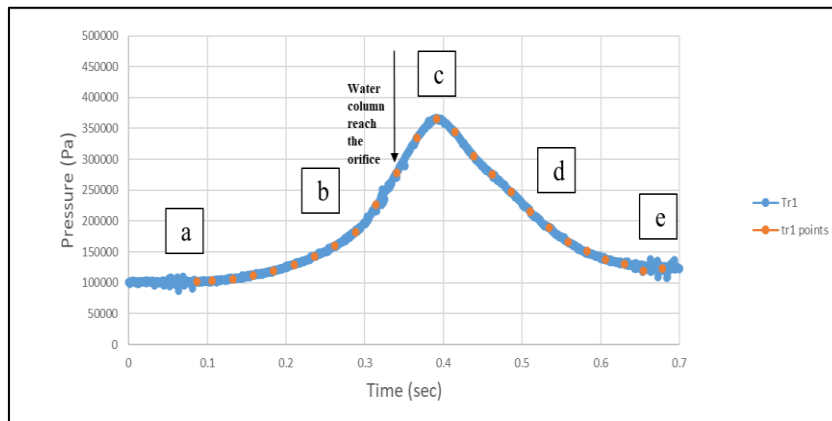

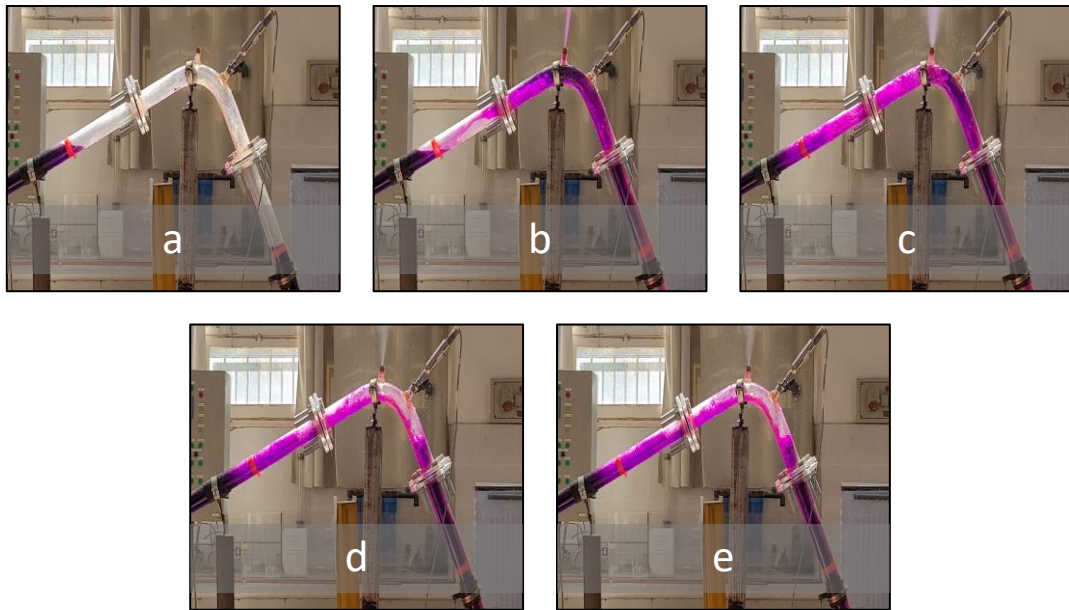**Figure 24**.1st cycle of air expulsion at P1 (d_o=3 mm).

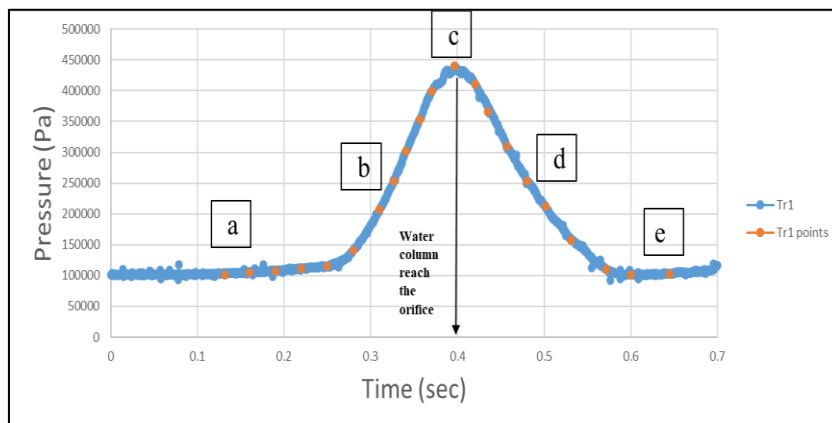**Figure 25**. illustration of air pocket expulsion at pocket 1 (d_o=3 mm).

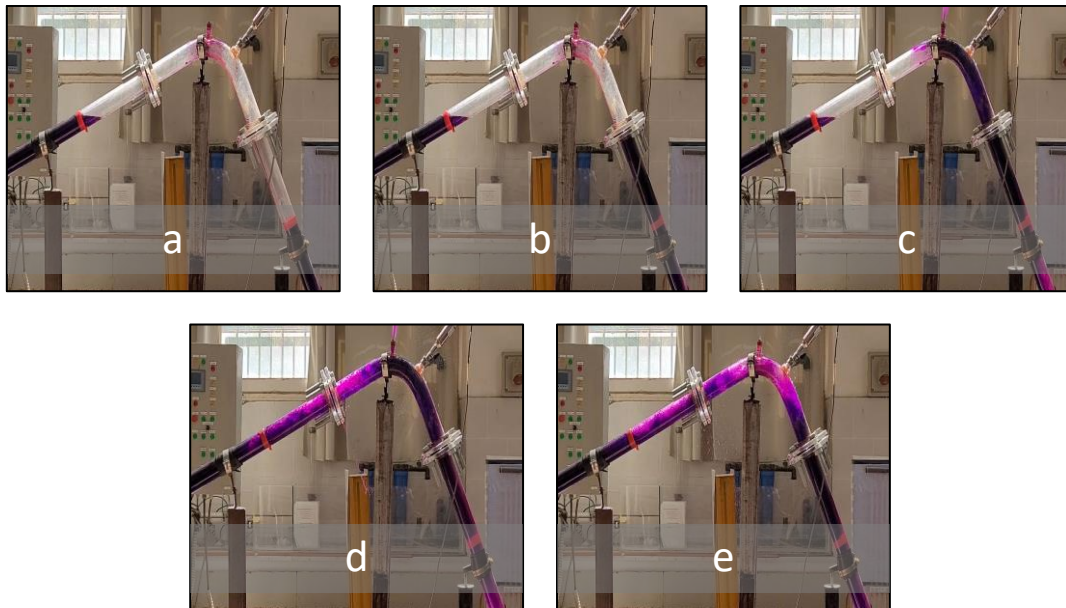**Figure 26**.1st cycle of air expulsion at P1 (d_o=7 mm).

Figure 27. illustration of air pocket expulsion at pocket 1 (d_o=7 mm).

Figures (22-27) showed a detailed observations of the air expulsion experiments at pocket 1 with air pocket size (L_{ao1}=100 cm) and the variation of orifice diameters (1.5-3-7 mm) were performed to observe the air pocket movement during both compression and expansion stages and focusing on the peak pressure in each case plotted on time frame Therefore for each case the graph is dotted for the 1st cycle of air pocket movement and the main points are highlighted and introduced in the illustration figures. Figures (22-23) describe the pressure pattern and images of air expulsion through small sized orifice (d_o=1.5 mm) where cushioning effect prevails. Figures (24-25) describe the pressure pattern and images of air expulsion through medium sized orifice (d_o=3 mm) where residual air is responsible for the peak pressure developed. Figures (26-27) describe the pressure pattern and images of air expulsion through small sized orifice (d_o=7 mm) where water hummer is dominated.

5. Conclusion

In the presented study, the air pocket entrapment and expulsion effect during rapid filling of irregular pipe are experimentally and numerically investigated. Numerical Results showed that the 2-D CFD model in ANSYS fluent using VOF method with (SST) k-ω turbulence model has validated the experimental data with reasonable agreement. Experiments observations by visualization of air pocket movement against pressure profiles showed more understanding of the phenomena of air entrapment with variety of air pocket size, blocking column length and air pocket location along the pipe as well as the air expulsion of air pocket with the variety of orifice diameter, air pocket size and location. Further future study could estimate the fluid structure interaction (FSI) effect in the numerical work.

6. Experiments and numerical uncertainty

6.1. Experimental uncertainty

The main sources of experimental uncertainty are accuracy of measuring devices which called systematic error and the random error due to the environmental instability during the experiments. In this study the systematic error is estimated according to manufacture specifications and random error is calculated for the measured pressure transducers at each location of air pocket. The results of each measured pressure are the average of (N) times repeated experiments to calculate the mean value (Ψ) where the standard deviations are calculated in the form:

$$S_\Psi = \sqrt{\frac{\sum_{i=1}^{N}(\Psi_i - \bar{\Psi})}{N-1}} \tag{11}$$

Where the random uncertainty in the form: -

$$S_{\bar{\Psi}} = \frac{S_\Psi}{\sqrt{N}} \tag{12}$$

The total uncertainty is the root sum of both random and systematic error calculation are in the following table:

Table 2. Parameters of experiments uncertainty calculations.

Measuring device	Unit	Range	System uncertainty (%)	Random uncertainty (%)	Total uncertainty (%)
Tank pressure gauge	bar	0–10	0.60	0.32	0.68
Pressure transducer	Psig	0-200	0.3	0.27	1.89

6.2. Numerical uncertainty

The estimated uncertainty in this study is calculated using The Grid Convergence Index (GCI) method [18] for the discretization of the governing equations. Three grids are computed as follows fine (563960 cell), medium (312630 cell), and coarse (179322 cell) for one air pocket case (Experiment#5 in Table 1) to compare the calculated error for pressure at the end of the pipe. Where the refinement ratio for each grid to another are fixed ($R_{21}=R_{32}$). the apparent accuracy order(q), the extrapolated value (Φ_{ext}^{21}) , the approximate relative error (e_a^{21}) , the extrapolated relative error (e_{ext}^{21}) and the GCI (GCI_{fine}^{21}) were calculated by the following equations: -

$$q = \frac{1}{ln(R_{21})}\left|ln\left|\frac{\Phi_3 - \Phi_2}{\Phi_2 - \Phi_1}\right|\right| \tag{13}$$

$$\Phi_{ext}^{21} = \frac{\Phi_1(R_{21})^q - \Phi_2}{(R_{21})^q - 1} \tag{14}$$

$$e_a^{21} = \left|\frac{\Phi_1 - \Phi_2}{\Phi_1}\right| \tag{15}$$

$$e_{ext}^{21} = \left|\frac{\Phi_{ext}^{21} - \Phi_2}{\Phi_1}\right| \tag{16}$$

$$GCI_{fine}^{21} = \frac{1.25 e_a^{21}}{(R_{21})^q - 1} \tag{17}$$

The calculations for numerical uncertainty are mentioned in the following table: -

Table 3. parameters of numerical uncertaintycalaculations.

Φ= Pressure peak calculated at end of the pipe (Pa)

n1-n2-n3	563960-312630-179322
$R_{32}=R_{21}$	1.3
Φ1-Φ2-Φ3	193629.341-194596.458-195164.059
q	1.8
Φ_{ext}^{21}	192255.335
e_a^{21}	0.71%
e_{ext}^{21}	0.49%
GCI_{fine}^{21}	0.88%

Nomenclature
- H_d = tank driving pressure
- A_0, A_1, A_2, A_3 = air valves along pipe
- D_{r0}, Dr_1, Dr_2, Dr_3 = drains point along pipe
- T_{r1}, Tr_2, Tr_3 = pressure transducers
- L_f = filling water column
- L_b = water blocking column length
- L_{ao1}, L_{ao2}, L_{ao3} = air pocket lengths for pocket one, two and three
- P1, P2, P3 = three air pocket locations
- d_o = orifice diameter
- L_T = total pipe length
- α = volume fraction (dimensionless)
- ω = turbulence specific dissipation rate (1/s)
- Γ_k = effective diffusivity of k (Kg/m. s)
- Γ_ω = effective diffusivity of ω (Kg/m. s)
- v = kinematic viscosity (m^2/s)
- t = time (s)
- ρ = density (kg / m^3)
- g = gravitational acceleration (m/s^2)
- k = turbulence kinetic energy (m^2/s^2)
- G_k = production of k (kg/m. s^3)
- G_ω = generation of ω (kg/m^3. s^2)
- Y_k = dissipation of k due to turbulence (kg/m. s^3)
- Y_ω = dissipation of ω due to turbulence (kg/m^3. s^2)
- D_ω = cross diffusion term (kg/m^3. s^2)
- u = velocity (m/s)
- a_l = speed of sound (m/s)

References

[1]   Chaudhry M H 1979 *Applied Hydraulic Transients* (Van Nostrand Reinhold New york)

[2]   Li L and Zhu D Z 2018 Modulation of transient pressure by an air pocket in a horizontal pipe with an end orifice *Water Science and Technology* **77** 2528-36

[3]   Martin C and CS M 1977 Entrapped air in pipelines *Proc. of the 2nd Int. Conf. of Pressure Surges* England 15–27

[4]   Aktershev S and Fedorov A 1987 Increase in water-hammer pressure in a pipe in the presence of a localized volume of gas *J. of Applied Mechanics and Technical Physics* **28** 899-903

[5]   Izquierdo J, Fuertes V, Cabrera E, Iglesias P and Garcia-Serra J 1999 Pipeline start-up with entrapped air *J. of hydraulic research* **37** 579-90

[6]   Fuertes V, Cabrera E, Izquierdo J and Iglesias P 1999 Peak pressure evaluation in pipelines with entrapped air pockets *Proc. of the 3rd ASME/JSME Joint Fluids Engineering Conf.* pp 18-23

[7]   Burrows R and Qiu D 1995 Effect of air pockets on pipeline surge pressure *Proc. of the Institution of Civil Engineers-Water Maritime and Energy* **112** 349-61

[8]   Zhou L, Liu D-y and Ou C-q 2011 Simulation of flow transients in a water filling pipe containing entrapped air pocket with VOF model *Engineering Applications of Computational Fluid Mechanics* **5** 127-40

[9]   Zhou L, Liu D and Karney B 2013 Investigation of hydraulic transients of two entrapped air pockets in a water pipeline *J.of Hydraulic Engineering* **139** 949-59

[10]   Holley E R 1969 Surging in laboratory pipeline with steady inflow *J.of the Hydraulics Division* **95** 961-80

[11]   Albertson M L and Andrews J 1971 Transients caused by air release Control of flow in closed conduits *J. P. Tullis ed. Colorado State Univ. Fort Collins Colo 315*-40

[12]   De Martino G, Fontana N and Giugni M 2008 Transient flow caused by air expulsion through an orifice *J. of Hydraulic Engineering* **134** 1395-9

[13]   Zhou L, Pan T, Wang H, Liu D and Wang P 2019 Rapid air expulsion through an orifice in a vertical water pipe *J. of Hydraulic Research* **57** 307-17

[14]   Zhou F, Hicks F and Steffler P 2002 Transient flow in a rapidly filling horizontal pipe containing trapped air *Journal of Hydraulic Engineering* **128** 625-34

[15]   Apollonio C, Balacco G, Fontana N, Giugni M, Marini G and Piccinni A F 2016 Hydraulic transients caused by air expulsion during rapid filling of undulating pipelines Water 8 25

[16]   Zhou L, Cao Y, Karney B, Bergant A, Tijsseling A S, Liu D and Wang P 2020 Expulsion of Entrapped Air in a Rapidly Filling Horizontal Pipe *J. of Hydraulic Engineering* **146** 04020047

[17]   Hirt C W and Nichols B D 1981 Volume of fluid (VOF) method for the dynamics of free boundaries *J. of computational physics* **39** 201-25

[18]   Engineers A S o M 2009 Standard for Verification and Validation in Computational Fluid Dynamics and Heat Transfer: An American National Standard: American Society of Mechanical Engineers)